

# Motion Processing Deficits in Children With Cerebral Visual Impairment and Good Visual Acuity

Arvind Chandna,<sup>1,2</sup> Nikolay Nichiporuk,<sup>1</sup> Spero Nicholas,<sup>1</sup> Ram Kumar,<sup>2</sup> and Anthony M. Norcia<sup>3</sup>

<sup>1</sup>Smith-Kettlewell Eye Research Institute, San Francisco, California, United States

<sup>2</sup>Alder Hey Children's Hospital, Liverpool, United Kingdom

<sup>3</sup>Stanford University, Stanford, California, United States

Correspondence: Arvind Chandna, Smith-Kettlewell Eye Research Institute, 2318 Fillmore Street, San Francisco, CA 94115, USA; [arvind@ski.org](mailto:arvind@ski.org).

**Received:** December 23, 2020

**Accepted:** September 1, 2021

**Published:** November 15, 2021

Citation: Chandna A, Nichiporuk N, Nicholas S, Kumar R, Norcia AM. Motion processing deficits in children with cerebral visual impairment and good visual acuity. *Invest Ophthalmol Vis Sci.* 2021;62(14):12. <https://doi.org/10.1167/iovs.62.14.12>

**PURPOSE.** We sought to characterize neural motion processing deficits in children with cerebral visual impairment (CVI) who have good visual acuity using an objective, quantifiable method (steady-state visual evoked potentials [SSVEPs]).

**METHODS.** We recorded SSVEPs in response to three types of visual motion – absolute motion and more complex relative and rotary motion, comparing them to form-related vernier and contour responses. We studied a group of 31 children with CVI diagnosed via detailed clinical examinations and 28 age-matched healthy controls.

**RESULTS.** Using measurements made at the appropriate response harmonics of the stimulation frequency, we found significant deficits in cerebral processing of relative and rotary motion but not of absolute motion in children with CVI compared with healthy controls. Vernier acuity, in keeping with good recognition acuity in both groups, was not different, nor were contour-related form responses.

**CONCLUSIONS.** Deficits for complex motion but relative sparing of elementary motion and form-related signals suggests preferential damage to extra-striate visual motion areas in children with CVI. The fact that these preferential losses occur in the absence of significant acuity loss indicates that they are not secondary to reduced visual acuity, but rather are an independent vulnerability in CVI. These results corroborate parental and caregivers' reports of difficulties with tasks that involve motion perception in children with CVI.

**Keywords:** cerebral visual impairment (CVI), relative motion, absolute motion, rotary motion, steady state visual evoked potentials (SSVEPs), visual acuity, dorsal stream dysfunction

Cerebral visual impairment (CVI) is the leading cause of childhood visual impairment in developed countries. Because its prevalence is rising in developing countries, it is now a major public health concern.<sup>1-3</sup> CVI commonly results from disruption to retrochiasmatic visual pathways and visual processing regions of the brain occurring during gestation, at delivery, or shortly thereafter.<sup>4</sup> The most common causes are perinatal hypoxia, hydrocephalus, and structural brain abnormalities. CVI is often associated with prematurity and comorbid cerebral palsy with periventricular leukomalacia, the most common brain lesion.<sup>5-9</sup>

CVI was previously diagnosed on the basis of reduced visual acuity alone in the presence of a normal ocular examination. This has limited the understanding of the condition. CVI has now been redefined as “A verifiable visual dysfunction, which cannot be attributed to disorders of the anterior visual pathways or any potentially co-occurring ocular impairment.” CVI encompasses a spectrum of visual and perceptual deficits collectively termed disorders of higher visual perceptual impairment or higher visual function deficits (HVFDs).<sup>7,10-14</sup> In essence, the diagnosis

of CVI is now a clinical diagnosis based on assessment of risk factors, exclusion of a purely ocular cause of the visual function impairment, supplemented when possible by other investigations, such as brain magnetic resonance imaging (MRI) scans. Normal visual acuity and absence or presence of brain MRI findings does not exclude a diagnosis of CVI.<sup>7,15</sup>

HVFDs may be the only symptomatology of children with good visual acuity in the presence of CVI.<sup>16-19</sup> In fact, a significant number of children with CVI who have good visual acuity remain undetected for higher visual function deficits, leading to significant difficulties in everyday life, school environments, and integration into society.<sup>10</sup> Higher visual functions (HVFs) are mediated by two putative cerebral networks; the “dorsal stream” connecting occipital and parietal lobes; and the ventral stream comprising occipital areas (e.g. V4) and temporal lobes.<sup>20,21</sup> HVFs, such as motion, dealing with complex visual scenes, navigation through three dimensional space and visually guided movements are assigned to the “where” or “action” dorsal stream, whereas color, shape, object, word, and face recognition are assigned to the “what” ventral stream.<sup>22-24</sup> Functionally,



there is considerable integration between the two streams to execute most visual functions, such as identification of objects and visually guided motion to reach and grasp.<sup>25</sup> In early life, functional morphology of the brain representing the dorsal stream is thought more vulnerable<sup>19</sup> resulting in a preponderance of dorsal stream deficits of HVFD in conditions leading to CVI.<sup>26</sup>

Alterations in motion perception are frequently observed by parents and teachers of children with CVI, as documented in structured history question inventories<sup>27–31</sup> and studied by psychophysical measurements that include biological form motion, optic flow fields (e.g. random dot kinematograms), and spatial integration tasks.<sup>14,32–34</sup> Most ambulant activities require accurate complex motion processing feeding onto the motor pathway for walking, reach and grasp, and avoidance of danger, such as avoiding traffic. The presence of these higher-order motion processing deficits suggests that specific testing for motion deficits using an objective method may yield high diagnostic value. Visual evoked potentials (VEPs) provide objective measures of brain function that promise to extend the possibility of a CVI diagnosis to earlier ages and nonverbal participants. Early work with VEPs has shown vernier acuity deficits,<sup>35,36</sup> spatial contrast sensitivity loss,<sup>37</sup> and translational and radial motion deficits.<sup>38</sup>

To the best of our knowledge, only one study has utilized VEPs to measure motion-related responses in children with CVI.<sup>39</sup> Children in this study had low visual acuity and a CVI diagnosis based on periventricular leukomalacia (PVL) associated with prematurity or hydrocephalus. In this study, Weinstein and co-workers<sup>39</sup> showed selective global (but not local) motion deficits. However, children diagnosed with CVI with normal or near-normal visual acuity were excluded from the study, but controls had normal visual acuity, so deficits in motion processing could have been secondary to visual acuity loss.

Here, we use the steady-state visual evoked potential (SSVEP) to study both simple and complex motion processing in children who have normal or near-normal visual acuity with a clinical diagnosis of CVI, as defined by Sakki and co-workers,<sup>11</sup> comparing them to neurotypical children. By studying children with near normal visual acuity, we focus on deficits that are not likely to be secondary to reduced stimulus visibility. As an internal control, we measure responses to form-related aspects of two of our stimuli in order to focus specifically on motion processing alterations. We find preserved processing of simple motion and to formed responses, but reduced responses to more complex types of motion in CVI, suggesting that complex motion processing deficits – a form of akinetopsia – can occur independently of acuity loss in children with CVI.

## METHODS

This research study was conducted in compliance with ethical approval obtained from the Alder Hey Children's Hospital Research Ethical Committee Reference 14/NW/1293. Informed consent was obtained from the parents and assent, where applicable, from the older child participant after explanation of the nature and possible consequences of the study.

## Participants

Thirty-one children (17 girls, mean age = 8.62 years, SD = 2.66; range = 4.4–14.53 years) with near-normal visual

acuity and CVI participated. They received a diagnosis of CVI based on an integrated assessment of gestational, birth and developmental history, detailed eye examination including cycloplegic refraction, oculomotor, and sensory status (author A.C. and Orthoptist), detailed neurologic examination, and review of neuroimaging for clinicoradiological diagnosis and symptom correlation (author R.K.), and MRI. These measures were obtained in almost all (31 out of 33) children. The results of MR brain imaging (31 children) were considered as supportive of the diagnosis but a normal MRI scan did not exclude a diagnosis of CVI.<sup>11,40–42</sup> The control group comprised 27 neurotypical children (16 girls, mean age = 9.06 years, SD = 3.02, range = 3.56–16.74 years). CVI-diagnosed children had best-corrected logMAR binocular visual acuities of mean 0.12 (SD = 0.11, range = –0.10 to 0.40, two children 0.30 or worse, and the remaining 29 children 0.20 or better); neurotypical children had binocular visual acuities of mean 0.14 (SD = 0.16, range = 0.00–0.20 logMAR). Neurotypical children had normal birth history, normal visual acuity, ocular examination, and motility, with better than 120 seconds of arc for stereopsis by TNO test and no health problems. For clinical details and MRI scan results in children diagnosed with CVI, see [Appendix A: Table 1](#) and [Table 2](#). Most children with CVI had more than one comorbid condition, similar to other studies of children with CVI.<sup>7,11,43,45</sup>

## Visual Display


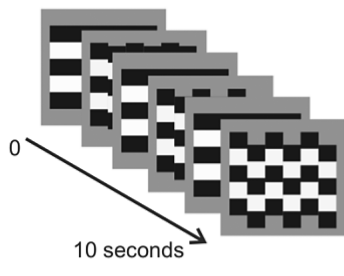
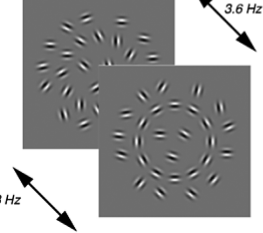
All stimuli were generated on a high bandwidth monochrome video monitor (Richardson Electronics MR2000-HB) at a resolution of 1600 × 1200 with a frame refresh rate of 60 Hz. Mean luminance was 155 cd/m<sup>2</sup>. The viewing distance was set at 100 cm, corresponding to a visual angle of 13.50 degrees × 14 degrees.

## Fast-Jitter Stimulus (Absolute Motion)

The spatial phase of a vertical sine wave grating (2 cpd, 80% contrast) was square-wave alternated to generate oscillatory motion over 0.5 to 7.5 arc minute at a temporal frequency of 7.5 Hz ([Fig. 1A](#)). Previous work has shown that the second (even) harmonic (2F; 15 Hz) registers a response to absolute motion.<sup>46</sup> We also analyzed the smaller fourth harmonic component (4F) for this study as it was readily measurable in the neurotypical children.

## Vernier Offset Stimulus (Relative Motion and Vernier Acuity)

[Figure 1B](#) illustrates the vernier offset stimulus that provided information on both relative motion and vernier offset responses. A series of spatial offsets was introduced and withdrawn periodically at 3.0 Hz from a collinear set of bars. The magnitude of the offsets was swept over a range of values spanning the perceptual threshold and beyond it (0.25 to 7.5 minutes arc). Previous work has shown that the odd harmonics (especially the first harmonic response, 1F) is specific to the relative form/position of the static and moving display elements (vernier response) and the even harmonics (and especially the second harmonic response, 2F) index responses to relative motion and local contrast changes, enabling SSVEP measures of two visual functions (vernier and relative motion) from one stimulus display.<sup>46,47</sup>

Stimulus Name	Stimulus Schematic	Response to Stimulus
<b>A</b> Fast Jitter (Absolute Motion)		<b>Absolute Motion</b> - Second (even) harmonic
<b>B</b> Vernier offset (Relative Motion and Vernier Acuity)		<b>Vernier Acuity</b> - First (odd) harmonic  <b>Relative Motion</b> - Second (even) harmonic
<b>C</b> Contour-in-Noise (Rotary Motion)		<b>Rotary Motion</b> - Even harmonics of background gabors

**FIGURE 1.** Stimulus schematics. **(A)** Fast jitter stimulus. The grating alternated between two positions at 7.5 Hz, with the size of the displacements being swept over 10 equal log values. A single value of displacement is illustrated. **(B)** Vernier offset stimulus (alignment/misalignment). Alternate panels of the bar grating alternated position at 3 Hz, with the other panels being static. A single value of displacement is illustrated. **(C)** Contour-in-noise paradigm. Contour elements were rotated at 3 Hz to either align with or be misaligned with the spine of an implicit circular contour. At the same time, randomly placed and oriented noise elements were rotated through the same angle at 3.6 Hz. There were seven contours at all times, with the noise density being swept from high to low values. A single value of noise density is illustrated.

### Contour-in-Noise Stimulus (Rotary Motion and Contour Responses)

The contour-in-noise stimulus (Fig. 1C) is comprised of two sets of Gabor patches – circular contours and randomly oriented “noise” elements. Each contour comprised 12 Gabor patches (contour elements) that lie along an implicit closed contour with constant spacing of four lambda between patches, where lambda is the wavelength of the Gabor carrier spatial frequency (5 c/degrees; Gabor patch standard deviation 0.5 degrees) There were seven circular contours spaced on a hexagonal grid. The contour elements, frequency tagged at 3 Hz, alternating between a closed circular contour shape with the orientation of each patch tangent to an implicit circle and a mis-aligned “sawblade” configuration in which each patch was rotated off the implicit contour by 60 degrees (collinear – non collinear) see Figure 1. This aspect of the display is similar to that used previously to measure VEPs.<sup>48</sup> The remainder of the Gabor patches were tagged at 3.6 Hz. These “noise” patches also rotated by 60 degrees, but had random carrier orientations and were never collinear. The density of the randomly located noise patches was systematically decreased over the trial, which in turn increased the visibility of the contour. The relative spac-

ing of the background element versus the contour elements varied between 0.57 (noise patch density higher than contour patch density) and 1 – equal density. This approach has been used previously with static Gabor patches to modulate contour visibility.<sup>49–53</sup>

### Procedure

Five GRASS 9 mm gold cup electrodes (model: E5GH) were placed according to the International 10–20 electrode placement system over the occipital pole at PO7, O1, Oz, O2, PO8, with the reference at Cz and ground at Pz.<sup>54,55</sup> Responses were recorded for each participant in a single session. A familiarization session was set up prior to proceeding with testing with the three stimulus conditions. Each stimulus condition consisted of six to ten 10 to 12 second trials and presentation order was randomized across conditions.

Most children sat on their own with their parents beside them; fixation was monitored constantly for all participants by the tester through a small cutout in a black screen that surrounded the monitor. Early in the course of the study, a remote video camera was introduced as an additional monitor for fixation for most (As the camera was introduced during the early part of the study, not all participants had

this additional monitoring. However, the mainstay of the monitoring of fixation was based on direct observation through the cutout for all participants). of the participants. All stimuli were viewed binocularly with spectacle correction, if prescribed. Attention to the stimulus was actively encouraged by a central cross fixation target, additional small toys dangling around the center, age-appropriate rhymes, and stories or the child's own favorite audiotape. The presentation was stopped if the experimenter judged a participant to not be paying attention and restarted upon re-engagement. Rest periods were given at regular intervals throughout the session.

### Electroencephalogram Data Analysis

Raw scalp potential records for each 10 to 12 second trial were sampled at 600 Hz (16-bit precision) and partitioned into 10 to 12 sequential epochs of 1-second duration (termed "bins"). Recursive least squares (RLS) spectrum analysis was used to determine SSVEP amplitude and phase for each bin at the relevant harmonic/s of the stimulus frequency.<sup>56</sup> Amplitude versus time (e.g. voltage versus swept parameter value) functions were obtained by coherently averaging across trials for each subject for each channel, relevant harmonic, and stimulus condition. Statistical significance was quantified using *P* values derived from the  $T^2_{circ}$  statistic,<sup>56</sup> a two-dimensional measure of variance-normalized mean amplitude and phase, distributed as  $F(2,2n-2)$ , where *n* is the number of trials (6–10 per condition).

### SSVEP Response Function Analysis

For each stimulus condition, amplitude versus time functions (stimulus-response functions) were fit with a sigmoidal function with four parameters (baseline, maximum excursion, sweep value at half maximal excursion, and an exponent controlling the steepness of the sigmoid; Equation 1). Error bars were estimated by boot-strapping, taking the standard deviation of 5000 random re-samplings of subjects with replacement within each participant group. The statistical significance of difference between the two groups at each level of independent variable (swept stimulus value) was evaluated by a *t*-test for two samples with unequal variance.

$$y = y_{min} + \frac{y_{max}}{1 + \left(\frac{x_{half}}{x}\right)^m} \quad (1)$$

### SSVEP Threshold Estimation and Analysis

Sensory thresholds were estimated by a regression to zero amplitude of the swept response function when the signal to noise ratio was adequate. Whereas the complete response function measures cortical processing over both sub- and suprathreshold parameter values, the threshold analysis informs us of the onset of a sensory response in visual cortex, providing important information about the threshold of visibility. The regression was based on the amplitudes from the trial-average epochs, where the response was measured over stimulus values that were of very low visibility to ones that were of high visibility. The range of epochs eligible for regression depended on the presence of statistically significant and phase-consistent responses according to an algorithm adapted from ref. 57. The regression range was limited to those epochs where the following criteria were met: (1) response *P* value in each bin was 0.16 or better;

(2) at least two consecutive bins anywhere within the range with  $P \leq 0.077$  or less; (3) the difference in response phase for each pair of consecutive bins was between  $-10$  and  $\pm 90$  degrees range from the phase at the preceding bin; and finally (4) the amplitude in any given bin could not be greater than 3.33 times the amplitude of the preceding bin in order to exclude a nonmonotonic rise. Once the regression range was established, the threshold stimulus value was determined by extrapolating the regression line to zero response amplitude. The thresholds estimated by the algorithm were manually inspected to correct for known failure modes when fitting response functions with very few signal-present measurements in the range. Thresholds were determined for each combination of harmonic, condition, and electrode across the two groups. The statistical significance between the two groups for each threshold was evaluated by a *t*-test for two samples with unequal variance.

### SSVEP Threshold Estimation Further Analysis of "Best Electrodes"

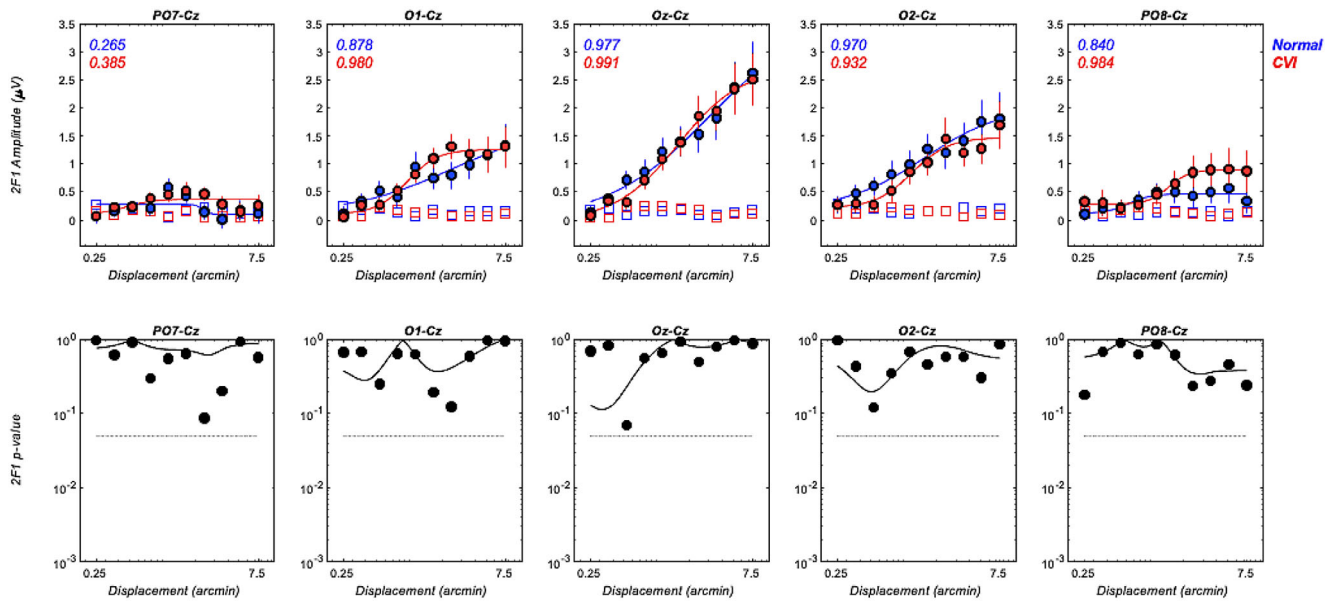
Traditionally in SSVEP studies, the best threshold measure is taken as evidence of the visual cortex having "seen" the stimulus. However, this method of threshold selection is open to outlier effects. To reduce outlier effects while still maintaining the robustness of the estimator, given the five-electrode array, both the best and second-best electrodes (which amounted to roughly the 75th percentile) were analyzed for each participant. We show a cumulative distribution function and a histogram of best and second-best thresholds for neurotypical children (blue) and children with CVI (red) in subsequent figures in the Results section. A two-sample *t*-test was used to compare the distributions.

## RESULTS

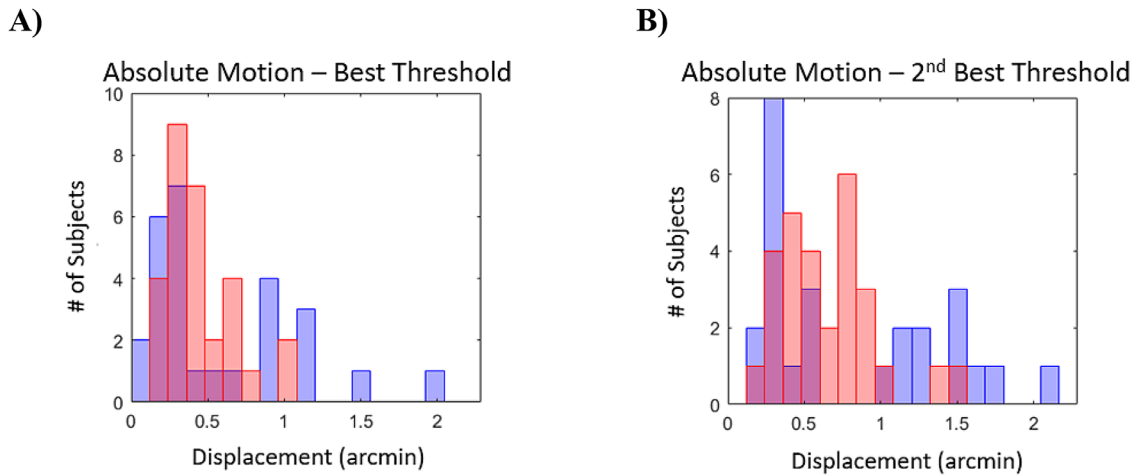
Each of the paradigms used in the present study involves measuring evoked-response amplitude as a function the value of the paradigm's swept parameter. Each paradigm can elicit evoked activity at one or more harmonics of each temporal frequency in the stimulus. Responses are not present at some harmonics, say, for example, odd harmonics of the absolute motion paradigm due to symmetry considerations. Responses at some harmonics can have low signal-to-noise ratio and thus are not reported. We thus focus the reporting on the harmonics that are expected from the design of the paradigm and of those that have adequate signal-to-noise ratio in all or some of the electrodes to be interpretable. Thresholds for the swept parameter are derived from these response functions as appropriate. In the figures, we display all five electrode responses if there are interpretable responses from the majority of electrodes.

Figure 2 shows the response amplitudes and significance criteria for the second harmonic response to the fast-jitter stimulus used to assess the integrity of responses to absolute motion (see Appendix B for the fourth harmonic fast-jitter harmonic responses). Each subpanel within the figure corresponds to one of the five electrodes spanning from the left hemisphere (PO7-Cz) to the right hemisphere (PO8). Data for the typically developing children are shown in blue and the responses for the children with CVI are shown in red.

The absolute motion response measured at 15 Hz is largest at Oz where it increases monotonically as a function of displacement, falling off rapidly at lateral electrodes



**FIGURE 2.** Absolute Motion. TOP: Group average response functions for absolute motion (displacement) at 2F. VEP amplitude versus displacement size is plotted for each of five electrodes (the three central electrodes show the best interpretable responses) for children with CVI (red) and age-matched neurotypical controls (blue). Open squares indicate the noise-level during the trial measured at frequencies adjacent to the response frequency. Goodness of fit of the sigmoid model is indicated in the upper left of each panel. BOTTOM: Each panel plots the result of two-sample *t*-tests for between-group differences at each sweep step (the three central electrodes are relevant). See Appendix B for fourth harmonic fast-jitter responses.



**FIGURE 3.** Absolute Motion. Histograms of best and second-best thresholds for absolute motion responses at the second harmonic among children with CVI (red) and healthy controls (blue). (A) Histogram for best achieved thresholds (mean CVI = 0.45 arcmin, mean control = 0.57 arcmin). The difference between the two groups is not significant,  $t(35.2) = 1.16, P = 0.25$ . (B) Histogram for second-best achieved threshold (mean CVI = 0.65 arcmin, mean control = 0.82 arcmin). The difference between the two groups is not significant,  $t(34.9) = 1.32, P = 0.19$ .

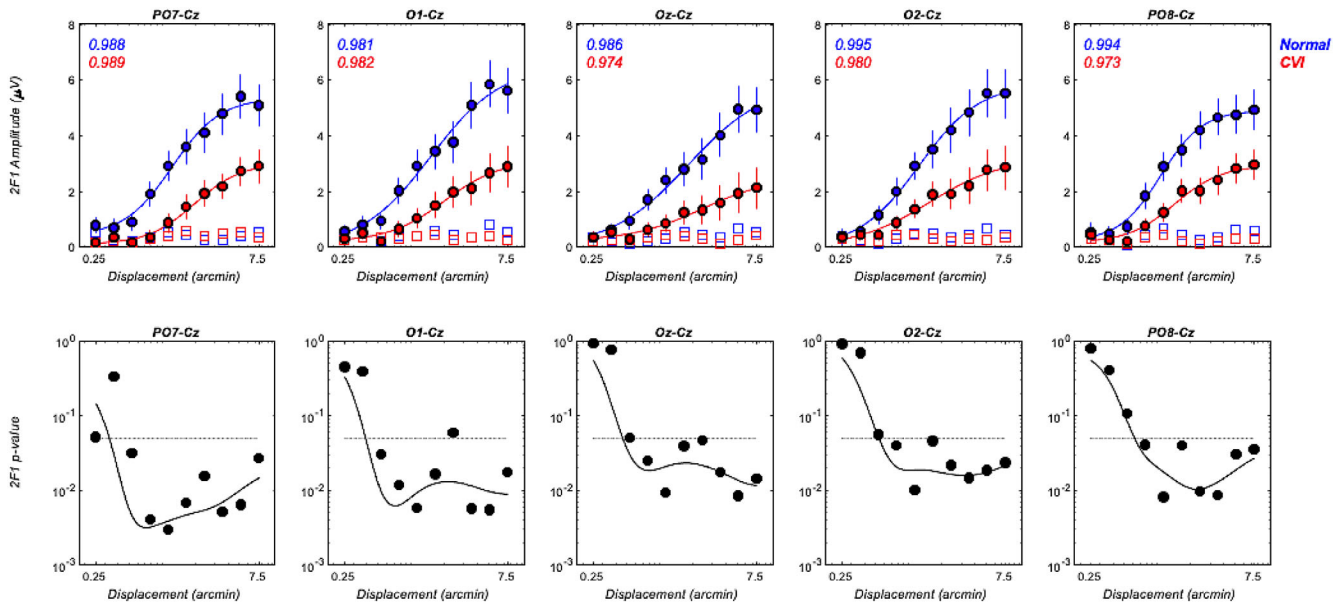
PO7 and PO8. The responses in the CVI group do not differ from those of the control group at any of the displacements measured (see lower panels - dotted line indicates  $P < 0.05$  significance level).

Absolute motion thresholds from the individual participant data records are shown as histograms of best and second-best thresholds in Figures 3A and 3B. Between the two groups there was no statistically significant difference for either the means of best (CVI group = 0.45 arcmin and the control group = 0.57 arcmin,  $t(35.2) = 1.16, P = 0.25$ ) or second best (0.65 arcmin for CVI versus 0.82 arcmin for controls:  $t(34.9) = 1.32, P = 0.19$ ) thresholds.

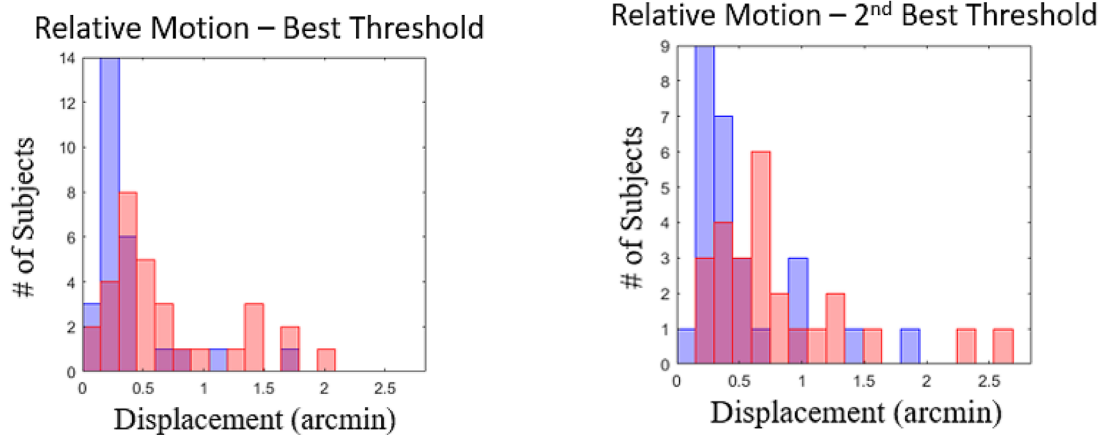
However, although thresholds for best and second best electrodes for neurotypical subjects were not significantly different ( $t(50) = -1.16, P = 0.1$ ); children with CVI did show a significant difference for best and second best electrodes ( $t(54) = -2.82, P = 0.006$ ).

**Relative Motion**

In contrast with the responses to absolute motion shown in Figure 2, responses to relative motion differ between groups, as can be seen in Figure 4. Responses to rela-



**FIGURE 4.** Relative Motion. TOP: Group average response functions for relative motion (displacement) response seen at the second harmonic (2F). VEP amplitude versus displacement size (0.25 to 7.5 min arc) is plotted for each of five electrodes for children with CVI (red) and neurotypical controls (blue). Open squares indicate the noise-level during the trial measured at frequencies adjacent to the response frequency. Goodness of fit of the sigmoid model is indicated in the upper left of each panel. BOTTOM: Each figure plots the result of two-sample *t*-tests for between-group differences at each sweep step; the 0.05 significance threshold (dotted line). See Appendix C for fourth harmonic responses.

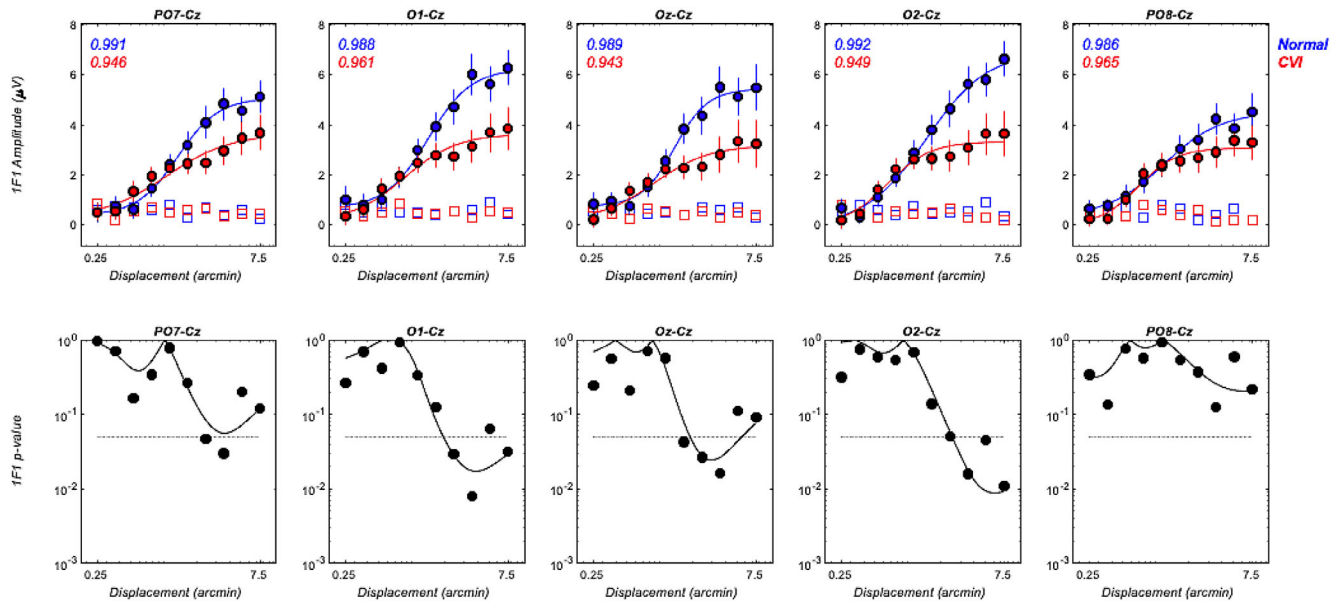


**FIGURE 5.** Relative motion thresholds. Histograms of best (A) and second-best thresholds (B) for relative motion responses at 2F among children with CVI (red) and healthy controls (blue). Children with CVI showed worse threshold values than neurotypical children. The second-best achieved thresholds showed similar results (mean CVI = 0.82 arcmin, mean control = 0.51 arcmin;  $t(49) = -2.20, P = 0.03$ ). However, no significant difference was found between the best and second-best thresholds within either group (CVI:  $t(54) = -0.88, P = 0.38$  and neurotypicals:  $t(51) = -1.34, P = 0.18$ ).

tive motion peak at 6 microvolts for neurotypical children, compared to approximately 3 microvolts for children with CVI. The amplitude difference between groups exceeds our 0.05 significance threshold (see dotted line; Fig. 4, bottom) at small displacement values (<1 arcmin) and continues to exceed the significance threshold throughout the suprathreshold response range. Note also that the response falls off more gradually toward lateral electrodes than for the absolute motion response (compare with Fig. 2), suggesting that the responses to absolute motion and relative motion

are generated from different underlying cortical sources. Appendix C presents the fourth harmonic responses.

The histograms for the best and second-best relative motion thresholds (see Figs. 4A, 4B) show that children with CVI had significantly worse thresholds compared to controls (0.69 arcmin versus 0.36 arcmin, respectively;  $t(56) = -2.70, P = 0.01$ ). The second best thresholds were also significantly higher in the children with CVI compared to the control group (0.82 arcmin versus 0.51 arcmin, respectively;  $t(49) = -2.20, P = 0.03$ ). No significant differences were found



**FIGURE 6.** Vernier displacement responses indexed by 1F response to vernier onset-offset paradigm. Responses rise out of the noise at the same displacement values, with the functions only differing at the largest displacement values. Open squares indicate the noise-level during the trial measured at frequencies adjacent to the response frequency. Goodness of fit of the sigmoid model is indicated in the upper left of each panel.

between the best and second-best thresholds within either group (CVI =  $t(54) = -0.88$ ,  $P = 0.38$  and neurotypicals =  $t(51) = -1.34$ ,  $P = 0.18$ ).

### Vernier/Position Sensitivity

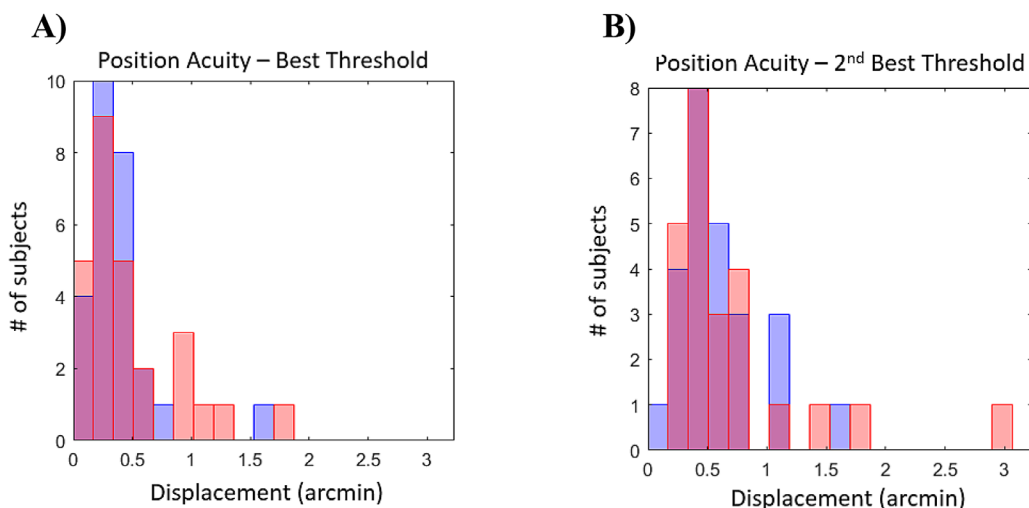
Whereas relative motion responses measured at the second harmonic (2F) are significantly different between neurotypical children and children with CVI throughout the range of displacements, the response measured for vernier offsets at the first harmonic (1F) does not differentiate the two groups at the smallest offset sizes and for more than half of the sweep range (see Fig. 6). Significant differences between groups occur only toward the end of the sweep (the seventh step; equivalent to 2.4 arcmin). The behavior of 1F and 2F at small offsets is thus very different, being affected at 2F and unaffected at 1F. Moreover, for 2F, there is a clear slope difference, with a bit of a lateral shift of the curve, but for 1F the curves have the same slope and offset and are very similar in amplitude for the two groups, up to the largest displacements. The portion of the 1F curves where the responses are equal is well above the experimental noise level, so the lack of a difference is not due to a floor effect. These results indicate that the alterations for smaller offsets seen for the simultaneously recorded second harmonic (see Fig. 4) are specific to, rather than being secondary to, reduced processing of form aspects of the vernier stimulus.

Figure 7 shows vernier acuity distributions, in arcminutes of stimulus displacement, for children with CVI and typically developing controls. The mean best threshold for children with CVI was 0.49 arcmin whereas for typically developing children the best threshold was 0.38 arcmin, a nonsignificant difference ( $t(51) = -1.16$ ,  $P = 0.25$ ). Similarly, no measurable difference was found for the mean second-best threshold (0.67 arcmin for CVI versus 0.59 arcmin for controls:  $t(36.2) = -0.61$ ,  $P = 0.25$ ). No significant difference was found between the best and second-best thresholds the

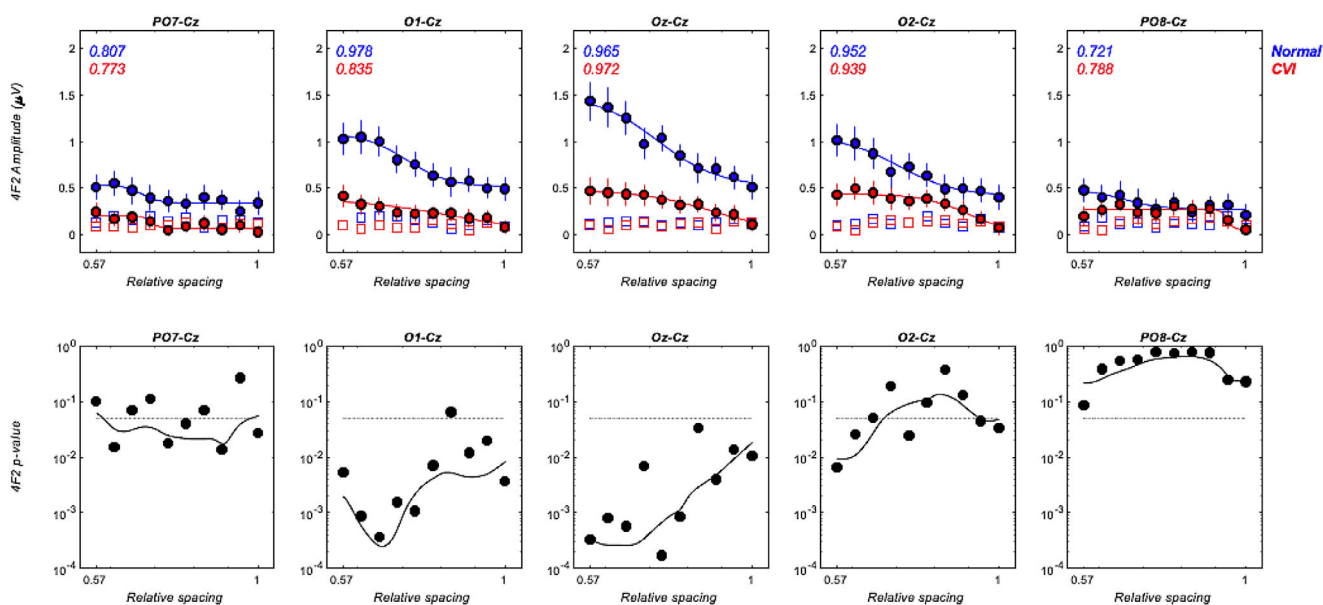
CVI group,  $t(49) = -1.23$ ,  $P = 0.22$ ; however, there was a significant difference between the mean best and second-best thresholds for the typically developing group,  $t(49) = -2.27$ ,  $P = 0.03$ .

### Rotary Motion Responses

In the contour and noise paradigm, the number of rotating “noise” Gabor elements starts at a high value and decreases over the duration of the response. The relative density thus changes between 0.57 and 1.0 over the course of the sweep trial. These display elements generate responses at even harmonics of the 3.6 Hz noise-element frequency (2F2 and 4F2). The responses to the noise patches are largest at low values of relative separation where the spacing of noise patches is smaller than that of the contour elements. Amplitudes measured at the fourth harmonic (e.g. at 14.4 Hz) begin at around 1.5 microvolts at Oz in the control children and drop in amplitude as the number of noise patches decreases (see Fig. 8 blue circles). A similar effect can be seen in the children with CVI, but their responses are much lower in amplitude. The reductions in response amplitude in the children with CVI differences are statistically reliable at O1 and Oz where the responses are largest (and at the beginning of the sweep for O2). Amplitudes for control group at small values of relative spacing (high noise density) were up to three times larger than those in children with CVI. The second harmonic 2F2 response at Oz is the same amplitude in both groups (see Appendix D) and this means that the 2F2 and 4F2 responses cannot be generated by the same process. Both are well-measured at Oz, so the lack of a difference is not likely a floor effect at 2F2. A possible model accounting for a dissociation of fourth and second harmonics is a cascade of two second order nonlinearities.<sup>58</sup> In such a model, the first stage generates activity at the second harmonic. This activity feeds the second stage that also comprises a second order nonlinearity. The output of



**FIGURE 7.** Vernier. Histograms of best and second-best thresholds for 1F position responses among children with CVI (*red*) and healthy controls (*blue*). **(A)** Histogram for best achieved thresholds (mean CVI = 0.49 arcmin, mean control = 0.38 arcmin, a nonsignificant difference:  $t(51) = -1.16, P = 0.25$ ). **(B)** Histogram for second-best achieved threshold (mean CVI = 0.67 arcmin, mean control = 0.59 arcmin, another nonsignificant difference  $t(36.2) = -0.61, P = 0.25$ ).



**FIGURE 8.** Rotary motion. TOP: Group average response functions for rotary motion (4F2) response. VEP amplitude versus density of surrounding Gabor patches is plotted for each of 5 electrodes for children with CVI (*red*) and age-matched neurotypical controls (*blue*). BOTTOM: Results of two-sample *t*-tests for between-group differences at each sweep step. Dotted line is  $P = 0.05$  significance criterion. Open squares indicate the noise-level during the trial measured at frequencies adjacent to the response frequency. Goodness of fit of the sigmoid model is indicated in the upper left of each panel. See Appendix D for second harmonic responses.

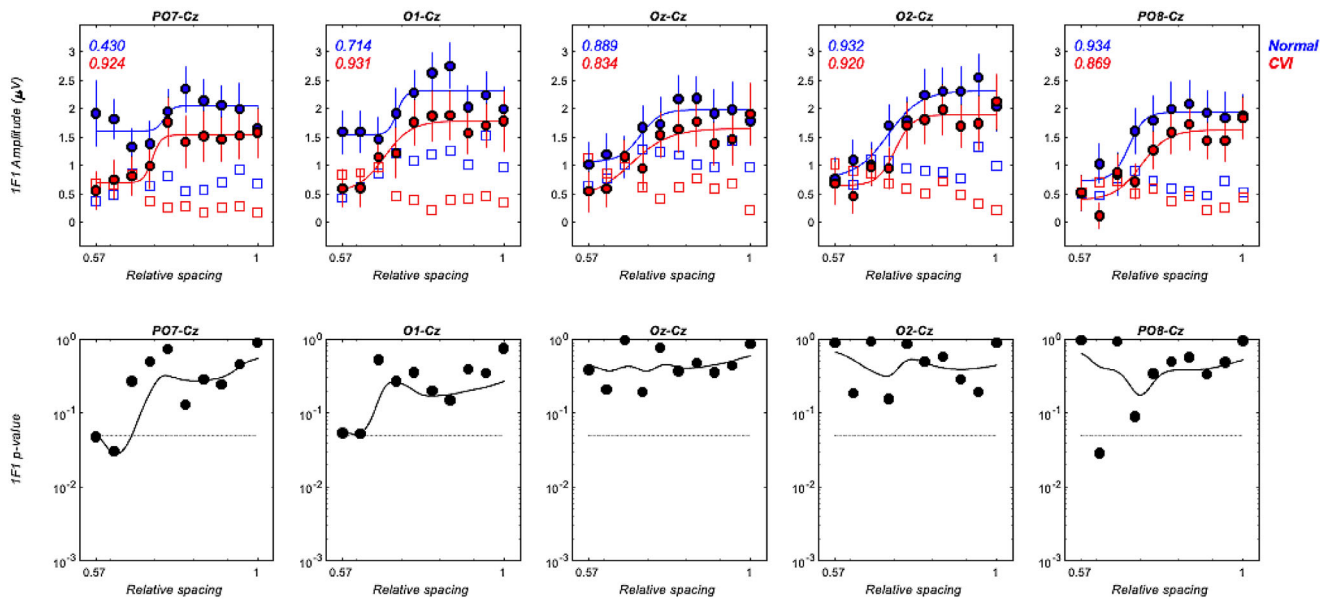
this stage is thus the fourth order with respect to the input (e.g. it generates a fourth harmonic). In this model, CVI preferentially effects the second, higher-order processing stage.

### Contour-Related Responses

The frequency tagging approach allows us to measure separate form-related responses that encode the alignment/misalignment of the Gabor patches with the spine of the implicit circular contours. These responses occur at odd harmonics of the contour-element modulation frequency of

3 Hz (1F1, 3F1, 5F1, etc.) and were measurable at 1F1. Group average functions for 1F1 are shown in Figure 9. Here, the responses to the constant number of contour elements increases as the number of noise patches decreases (relative density goes to 1). Responses are above the noise level on O2-Cz and PO8-Cz derivations for both children with CVI and age-matched neurotypical controls. No measurable differences were present on any of the five recording channels (see Fig. 9 bottom). The signal-to-noise ratio of individual participant data was too low to reliably estimate thresholds for the contour-related responses.





**FIGURE 9.** Contour response. TOP: Group average response functions for contour-related (1F1) responses. VEP amplitude versus density of surrounding Gabor patches is plotted for each of five electrodes for children with CVI (red) and age-matched neurotypical controls (blue). BOTTOM: Results of two-sample *t*-tests for between-group differences at each sweep step. Dotted line is  $P = 0.05$  significance criterion. No significant differences are present beyond those expected on repeated testing. Open squares indicate the noise-level during the trial measured at frequencies adjacent to the response frequency. Goodness of fit of the sigmoid model is indicated in the upper left of each panel.

Rotation of the contour elements also generates motion/transient responses at 2F1 (6 Hz) and 4F1 (12 Hz) in the same way that the noise elements generate responses at 2F2 (7.2 Hz; Appendix D) and 4F2 (14.4 Hz; see Fig. 8). The 2F1 and 4F1 responses from the contour elements increase in amplitude as the density of the noise elements decrease (Fig. 10, first and third rows). As was the case for 2F2 and 4F2 responses of the noise elements, these responses are smaller in the CVI group especially at the fourth harmonic (4F1). The observation that 1F1 (see Fig. 9), 2F1, and 4F1 responses increase as noise density decreases suggests that these contour-element related responses are each being released from spatial masking. The fact that form-related 1F1 response to the contour is not measurably different between groups but the motion/transient related responses are (at 4F1 and to a lesser extent at 2F1) suggests a relative sparing of form processing in the CVI group.

## DISCUSSION

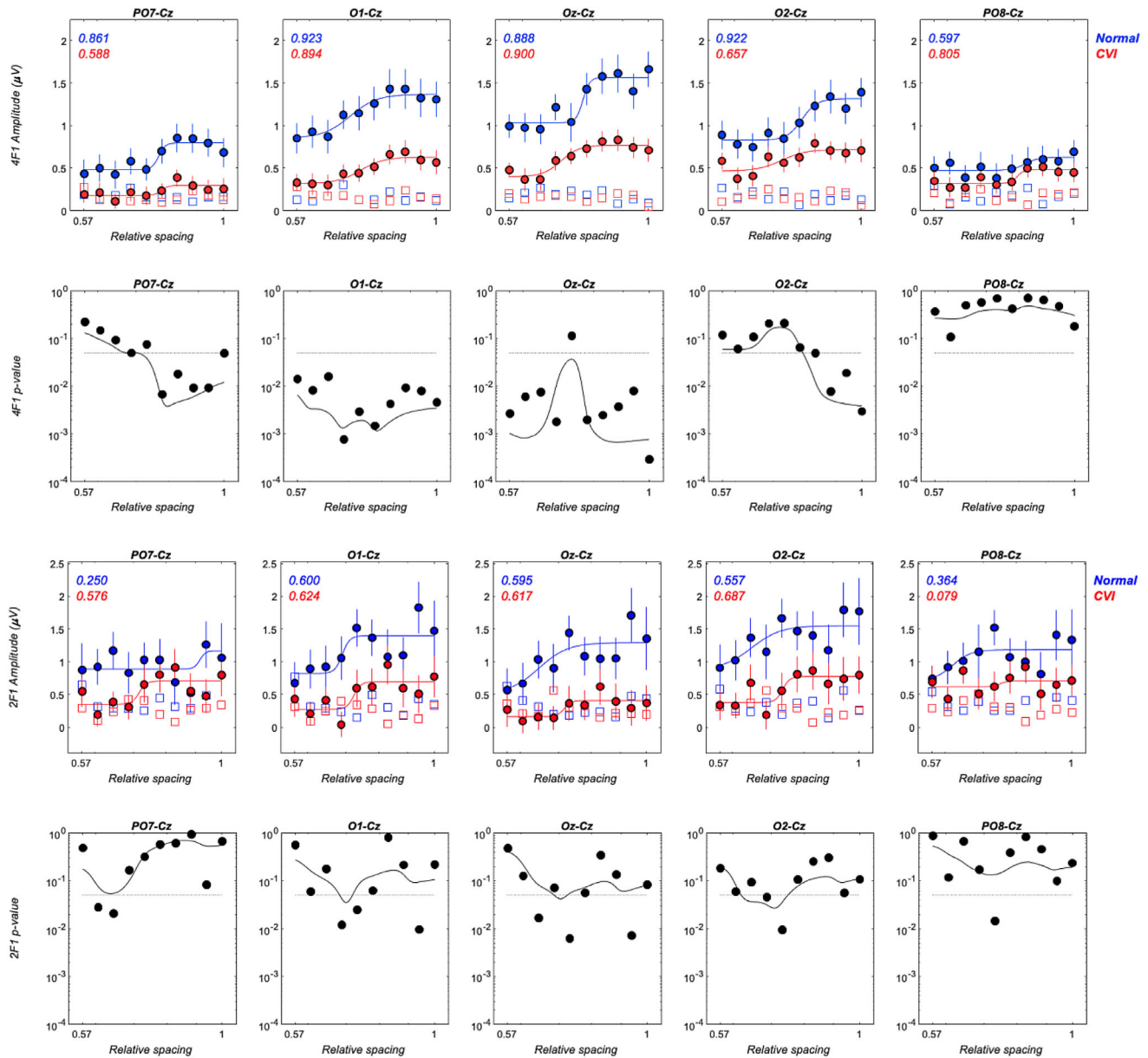
This is the first prospective, controlled study to characterize motion processing deficits in children with an established clinical diagnosis of CVI and good visual acuity using a direct neural measure, the SSVEP. Our results show that children with CVI have deficits in even harmonic responses in the vernier and contour-in-noise paradigms, but not in the absolute motion paradigm. That these processing differences preferentially involve more complex forms of motion processing is borne out by our observation that form related first harmonic responses measured at the same time in the vernier and contour paradigms are relatively unaffected. In the case of the contour-in-noise paradigm, even harmonic responses to the contour elements themselves are affected, despite the odd-harmonic responses being not measurably different. Depression of the contour-related even harmonic

responses may reflect preferential crowding of motion *vs* form processes when the density of the noise patches is high. Absolute motion, a simpler type of motion, is unaffected in our measurements.

It is likely that the even harmonic responses reflect – at least in part – the activity of motion rather than local contrast-change mechanisms. In the case of the absolute motion condition, this response is subject to direction-specific adaptation.<sup>58</sup> Moreover, this stimulus elicits the monocular developmental motion asymmetry in the VEP.<sup>59</sup> These past results suggest that even harmonic responses from this paradigm at least partially tap activity from direction-selective motion mechanisms in early visual cortex. In the future, it would be useful to rule out temporal frequency (e.g. 7.5 Hz versus 3 Hz) as the factor that spares the response to the oscillating grating compared to the other motion types.

Evidence for a motion contribution to the vernier second harmonic is less direct. The original publication on the vernier VEP paradigm used here<sup>46</sup> showed that both 1F and 2F thresholds were in the hyper-acuity range and that both had a steep eccentricity dependence typical of other hyper-acuities. The fine thresholds and steep eccentricity dependence of the vernier 2F response suggest that it is not primarily a response to local contrast change which would be expected to be less dependent on eccentricity.<sup>60</sup>

The involvement of direction-selective (motion) processes in the generation of even harmonics in the contour-in-noise paradigm is unknown, as this type of motion has not been studied neurophysiologically. Nonetheless, these even harmonic responses are preferentially affected in CVI. Analogous to the responses to the vernier stimulus, even harmonics from the contour elements are preferentially reduced in amplitude compared to the first harmonics from the same elements, consistent



**FIGURE 10.** Contour-element rotary motion responses. Group average response functions for rotary-motion 2F1 (*top*); and 4F1 (*bottom*) responses. VEP amplitude versus density of surrounding Gabor patches is plotted for each of five electrodes for children with CVI (*red*) and age-matched neurotypical controls (*blue*). *Open squares* indicate the noise-level during the trial measured at frequencies adjacent to the response frequency. Goodness of fit of the sigmoid model is indicated in the upper left of each panel. The *bottom panel* for 2F1 and 4F1 plot the result of two-sample *t*-tests for between-group differences at each sweep step. The *dotted line* is  $P = 0.05$  significance criterion. See text for details.

with a relative sparing of form processing in both paradigms.

Our results are consistent with prior results suggesting that CVI preferentially damages more complex motion processing mechanisms, while sparing simpler ones.<sup>31,35,44</sup> Importantly, we show that these losses occur in the relative absence of visual/vernier acuity and contour-integration deficits and are thus preferential to the motion pathway. Guzetta and co-workers<sup>34</sup> reported reduced behavioral responses to complex motion stimuli (segmented motion) in children with normal visual acuity born prematurely with PVL compared to a similar cohort of children without PVL lesions, indicating that higher-order motion perception is affected in children at higher risk of CVI (prematurity

and PVL) independent of visual acuity. Our results provide electrophysiological evidence for the psychophysical deficits of motion abnormality in their cohort. Weinstein and co-workers<sup>39</sup> showed selective global (but not local) motion deficits in children diagnosed with CVI based on presence of PVL lesions associated with prematurity or hydrocephalus, children with CVI with normal visual acuity were excluded from their study, but controls had normal visual acuity, so deficits in motion processing could have been secondary to visual acuity loss. Taken together, our results are consistent with patterns of differential loss of higher-order motion perception in patients with preserved pre-striate and striate areas but damage to extrastriate dorsal stream areas.<sup>19,61–63</sup>

Our objective results corroborate reports of a spectrum of perceptual motion processing difficulties documented with structured question inventories that have included questions aimed at assessing dorsal stream motion processing dysfunction.<sup>4,30,31,64</sup> An inability to see moving objects, such as cars on a road, while the child is stationary or an inability to spot animals in a field while the child is seated in a moving car are frequently reported, especially when the visual environment has multiple features. Dutton and co-workers<sup>65</sup> used structured questionnaire to study 40 children with clinical diagnosis of CVI due to multiple etiologies, similar to our study. In their group, 31 had 6/12 (20/40) or better binocular visual acuity; in 13 children, parents had observed impaired ability to see moving objects while stationary and all 40 had impaired visually guided motion. Our results demonstrating relative and rotary motion abnormalities are possibly related to these behavioral observations.

We also report that two form-related responses – the first harmonics of the vernier onset-offset and contour-alignment/misalignment responses (see Figs. 6, 7, 9, respectively) are relatively undisturbed in our CVI group. The vernier-related response is not measurably different at small offsets and the derived vernier acuity does not differ between groups (see Fig. 7). By contrast, responses at the second harmonic (2F) from the same stimulus are right-ward shifted and 2F thresholds are higher in the children with CVI, suggesting a relative sparing of form processing mechanisms. Vernier-related responses do, however, differ at large offsets, suggesting that any sparing of form processing is relative rather than absolute. VEP vernier acuity is correlated with logMAR acuity loss in amblyopia<sup>66</sup> and these points of concordance suggest that vernier acuity provides a surrogate for recognition acuity and thus may serve as a useful early predictor of recognition acuity in preverbal children unable to perform traditional behavioral recognition acuity. The first harmonic of the contour-related response does not differ between groups in our measurements, but even harmonic responses related to both the contour and noise elements do differ, again suggesting a relative sparing of form-related processes.

CVI diagnosis encompasses children in which CVI was likely caused by a range of different brain lesions that can be detected on neuro-imaging and a spectrum of functional deficits that are either directly or indirectly related to these structural abnormalities. Because of the nature of the diagnosis, there are comorbidities in our cohort of children that could influence the pattern of results.<sup>11</sup> For example, in our group, only 5 of 31 children had normal brain MRIs and only 7 of 31 did not have strabismus. The question is then which functional alterations are secondary to the comorbidities and which are in some sense “primary” to CVI. Our sample is too small to make a statement about the effects on the different VEP measures in a group of children without CVI who do not have strabismus or who did not have brain abnormalities on MRI. This question has at least partially been addressed in a study of coherent motion VEPs<sup>39</sup> where it was concluded that alterations of the VEP were more pronounced in children with CVI and strabismus than they were in otherwise healthy children with strabismus. Similarly, motion processing deficits, including a differential loss for higher levels of motion perception, including biological motion, have been reported in children born prematurely; with CVI<sup>67,68</sup> and without CVI<sup>34,69,70</sup> with the addition of CVI inducing greater loss. What we show here is a pattern of relative sparing and

deficit over multiple functional measures in a high visual acuity CVI population.

In children with CVI, normal MRI scans in the presence of abnormal neurology and vice versa are seen in this and other studies. Limitations of resolution in routine clinical MRI scans suggest that absence of abnormalities<sup>41,42</sup> or indeed a normal MRI postdating an abnormal cranial ultrasound does not exclude CVI.<sup>71</sup> Increasingly, arguments are being made for inclusion of additional supportive evidence of CVI. These include macro and micro-level structural brain abnormalities, attention deficits, visual perceptual spatial processing deficits, and other learning disorders with or without visually guided motor deficits.<sup>13,72,73</sup> The possible influence of additional comorbidities in our population, such as autism, strabismus, and amblyopia, are mitigated by the consistency of diagnosis of CVI for the entire study cohort whereas the comorbid conditions are sporadic. Nonetheless, much remains to be done to tease out the spectrum of visual deficits in children with CVI and the influence of comorbid conditions.<sup>74,75</sup>

## CONCLUSION

SSVEPs generated by a battery of different visual stimuli show evidence of specific motion processing deficits in the absence of visual acuity or visual form deficits. The high signal-to-noise ratio of the technique allows for the measurement of more than one visual dysfunction within individual patients, making this methodology suitable for further studies of the natural history of motion perception and form processing deficits in CVI and possibly determining outcomes of targeted (re)habilitative intervention.

## Acknowledgments

The authors thank the children and parents who participated as volunteers in the study. We thank Sylwia Migas, PhD for help with collection of data; Devashish Singh, Research Assistant, for his input; Laurence Abernethy, Neuroradiologist, for information on brain imaging, and members of the eye department Alder Hey Children's Hospital, UK, for assisting in recruitment and support for the study. We gratefully acknowledge the hard work of Nikolay Nichiporuk, who passed away prior to the submission of this paper.

Supported by ongoing grants for CVI research from vision4children (The Littler Trust) UK; Iceland Foods Charitable Foundation (UK), a SKERI grant to A.C. (USA), and a RERC grant (90RE5024-01-00; USA).

Disclosure: **A. Chandna**, None; **N. Nichiporuk**, None; **S. Nicholas**, None; **R. Kumar**, None; **A.M. Norcia**, None

## References

- Colenbrander A. What's in a name? Appropriate terminology for CVI. *J Vis Impair Blind*. 2010;104:583–585.
- Kong L, Fry M, Al-Samarraie M, Gilbert C, Steinkuller PG. An update on progress and the changing epidemiology of causes of childhood blindness worldwide. *J Am Assoc Ped Ophthalmol Strabismus*. 2012;16(6):501–507.
- Solebo AL, Teoh L, Rahi J. Epidemiology of blindness in children. *Arch Dis Childhood*. 2017;102(9):853–857.
- Dutton GN. The spectrum of cerebral visual impairment as a sequel to premature birth: an overview. *Documenta Ophthalmologica*. 2013;127(1):69–78.

5. Afshari MA, Afshari NA, Fulton AB. Cortical visual impairment in infants and children. *Int Ophthalmol Clin*. 2001;41(1):159–169.
6. Khetpal V, Donahue SP. Cortical visual impairment: etiology, associated findings, and prognosis in a tertiary care setting. *J Am Assoc Ped Ophthalmol Strabismus*. 2007;11(3):235–239.
7. Fazzi E, Signorini SG, Bova SM, et al. Spectrum of visual disorders in children with cerebral visual impairment. *J Child Neurol*. 2007;22(3):294–301.
8. Good WV. Cortical visual impairment: new directions. *Optom Vis Sci*. 2009;86:663–665.
9. Rahi JS, Gilbert CE. Epidemiology and world-wide impact of visual impairment in children. *Pediatric ophthalmology and strabismus*. 4th ed. New York, NY: Elsevier; 2012; 1–8.
10. Merabet LB, Mayer DL, Bauer CM, Wright D, Kran BS. Disentangling how the brain is “wired” in cortical (cerebral) visual impairment. In: *Seminars in pediatric neurology* (Vol. 24, No. 2, pp. 83–91). New York, NY: WB Saunders; 2017 May.
11. Sakki HEA, Dale NJ, Sargent J, Perez-Roche T, Bowman R. Is there consensus in defining childhood cerebral visual impairment? A systematic review of terminology and definitions. *Br J Ophthalmol*. 2018;102(4):424–432.
12. Lueck AH. Cortical or cerebral visual impairment in children: A brief overview. *J Vis Impair Blindness*. 2010;104(10):585–592.
13. Philip SS, Dutton GN. Identifying and characterising cerebral visual impairment in children: a review. *Clin Exp Optom*. 2014;97(3):196–208.
14. Boot FH, Pel JJM, van der Steen J, Evenhuis HM. Cerebral Visual Impairment: which perceptive visual dysfunctions can be expected in children with brain damage? A systematic review. *Res Dev Disabil*. 2010;31(6):1149–1159.
15. Bassan H, Limperopoulos C, Visconti K, et al. Neurodevelopmental outcome in survivors of periventricular hemorrhagic infarction. *Pediatrics*. 2007;120(4):785–792.
16. Dutton GN. Cognitive vision, its disorders and differential diagnosis in adults and children: knowing where and what things are. *Eye*. 2003;17:289–304.
17. Fazzi E, Bova SM, Uggetti C, et al. Visual-perceptual impairment in children with periventricular leucomalacia. *Brain Dev*. 2004;26:506–512.
18. Stiers P, Vanderkelen R, Vanneste G, Coene S, De Ramaelaere M, Vandebussche E. Visual-perceptual impairment in a random sample of children with cerebral palsy. *Dev Med Child Neurol*. 2002;44:370–382.
19. Braddick O, Atkinson J, Wattam-Bell J. Normal and anomalous development of visual motion processing: motion coherence and ‘dorsal-stream vulnerability’. *Neuropsychologia*. 2003;41:1769–1784.
20. Felleman DJ, Van Essen DC. Distributed hierarchical processing in the primate cerebral cortex. *Cereb Cortex*. 1991;1(1):1–47.
21. Young MP. Objective analysis of the topological organization of the primate cortical visual system. *Nature*. 1992;358(6382):152–155.
22. Milner AD, Goodale MA. Two visual systems re-viewed. *Neuropsychologia*. 2008;46(3):774–785.
23. Mishkin M, Ungerleider LG, Macko KA. Object vision and spatial vision: two cortical pathways. *Trends Neurosci*. 1983;6:414–417.
24. Milner AD, Goodale MA. Oxford psychology series, No. 27. The visual brain in action. 1995. Available at: [https://www.researchgate.net/publication/228744443\\_The\\_Visual\\_Brain\\_in\\_Action](https://www.researchgate.net/publication/228744443_The_Visual_Brain_in_Action).
25. Milner AD. How do the two visual streams interact with each other?. *Exp Brain Res*. 2017;235(5):1297–1308.
26. Macintyre-Béon C, Young D, Dutton GN, et al. Cerebral visual dysfunction in prematurely born children attending mainstream school. *Documenta Ophthalmologica*. 2013;127(2):89–102.
27. Gorrie F, Goodall K, Rush R, Ravenscroft J. Towards population screening for cerebral visual impairment: validity of the five questions and the CVI questionnaire. *PLoS One*. 2019;14(3):e0214290.
28. Hellgren K, Jacobson L, Frumento P, et al. Cerebral visual impairment captured with a structured history inventory in extremely preterm born children aged 6.5 years. *J AAPOS*. 2020;24(1):28.e1–28.e8.
29. Jackel B, Wilson M, Hartmann E. A survey of parents of children with cortical or cerebral visual impairment. *J Vis Impair Blindness*. 2010;104(10):613–623.
30. Macintyre-Beon C, Young D, Calvert J, Ibrahim H, Dutton GN, Bowman R. Reliability of a question inventory for structured history taking in children with cerebral visual impairment. *Eye*. 2012;26(10):1393–1393.
31. Ortibus E, Laenen A, Verhoeven J, et al. Screening for cerebral visual impairment: value of a CVI questionnaire. *Neuro-pediatrics*. 2011;42(04):138–147.
32. Atkinson J. The Davida teller award lecture, 2016: visual brain development: a review of “dorsal stream vulnerability”—motion, mathematics, amblyopia, actions, and attention. *J Vis*. 2017;17(3):26–26.
33. Pavlova M, Staudt M, Sokolov A, Birbaumer N, Krägeloh-Mann I. Perception and production of biological movement in patients with early periventricular brain lesions. *Brain*. 2003;126(3):692–701.
34. Guzzetta A, Tinelli F, Del Viva MM, et al. Motion perception in preterm children: role of prematurity and brain damage. *Neuroreport*. 2009;20(15):1339–1343.
35. Skoczenski AM, Good WV. Vernier acuity is selectively affected in infants and children with cortical visual impairment. *Dev Med Child Neurol*. 2004;46(8):526–532.
36. Watson T, Orel-Bixler D, Haegerstrom-Portnoy G. Early Visual Evoked Potential Acuity and Future Behavioral Acuity in Cortical Visual Impairment. *Optom Vis Sci: Official Publication of the American Academy of Optometry*. 2010;87(2):80.
37. Good WV, Hou C, Norcia AM. Spatial contrast sensitivity vision loss in children with cortical visual impairment. *Invest Ophthalmol Vis Sci*. 2012;53(12):7730–7734.
38. Kuba M, Liláková D, Hejčmanová D, Kremláček J, Langrová J, Kubová Z. Ophthalmological examination and VEPs in preterm children with perinatal CNS involvement. *Documenta Ophthalmologica*. 2008;117(2):137–145.
39. Weinstein JM, Gilmore RO, Shaikh SM, et al. Defective motion processing in children with cerebral visual impairment due to periventricular white matter damage. *Dev Med Child Neurol*. 2012;54(7):e1–e8.
40. Boot FH, Pel JJ, van der Steen J, et al. Cerebral visual impairment: which perceptive visual dysfunctions can be expected in children with brain damage? A systematic review. *Res Dev Disabil*. 2010;31:1149–1159.
41. Ortibus E, Lagae L, Casteels I, Demaerel P, Stiers P. Assessment of cerebral visual impairment with the I94 visual perceptual battery: clinical value and correlation with MRI findings. *Dev Med Child Neurol*. 2009;51(3):209–217.
42. Fazzi E, Bova S, Giovenzana A, Signorini S, Uggetti C, Bianchi P. Cognitive visual dysfunctions in preterm children with periventricular leukomalacia. *Dev Med Child Neurol*. 2009;51(12):974–981.
43. van Genderen M, Dekker M, Pilon F, Bals I. Diagnosing cerebral visual impairment in children with good visual acuity. *Strabismus*. 2012;20(2):78–83.
44. Jacobson L, Hård AL, Svensson E, Flodmark O, Hellström A. Optic disc morphology may reveal timing of insult in children with periventricular leukomalacia and/or periventricular hemorrhage. *Br J Ophthalmol*. 2003;87(11):1345–1349.

45. Bosch DG, Boonstra FN, Willemsen MA, Cremers FP, de Vries BB. Low vision due to cerebral visual impairment: differentiating between acquired and genetic causes. *BMC Ophthalmology*. 2014;14(1):59.
46. Norcia AM, Wesemann W, Manny RE. Electrophysiological correlates of vernier and relative motion mechanisms in human visual cortex. *Visual Neuroscience*. 1999;16(6):1123–1131.
47. Chen SI, Norcia AM, Pettet MW, Chandna A. Measurement of position acuity in strabismus and amblyopia: Specificity of the vernier VEP paradigm. *Invest Ophthalmol Vis Sci*. 2005;46(12):4563–4570.
48. Norcia AM, Sampath V, Chuan H, Pettet MW. Experience-expectant development of contour integration mechanisms in human visual cortex. *J Vis*. 2005;5(2):3.
49. Kozma P, Kiorpes L. Contour integration in amblyopic monkeys. *Visual Neuroscience*. 2003;20(5):577.
50. Kovács I, Polat U, Pennefather PM, Chandna A, Norcia AM. A new test of contour integration deficits in patients with a history of disrupted binocular experience during visual development. *Vis Res*. 2000;40(13):1775–1783.
51. Chandna A, Pennefather PM, Kovács I, Norcia AM. Contour integration deficits in anisometropic amblyopia. *Invest Ophthalmol Vis Sci*. 2001;42(3):875–878.
52. Chandna A, Gonzalez-Martin JA, Norcia AM. Recovery of contour integration in relation to LogMAR visual acuity during treatment of amblyopia in children. *Invest Ophthalmol Vis Sci*. 2004;45(11):4016–4022.
53. Williams C, Gilchrist ID, Fraser S, et al. Normative data for three tests of visuocognitive function in primary school children: cross-sectional study. *Br J Ophthalmol*. 2015;99(6):752–756.
54. Nuwer MR, Comi G, Emerson R, et al. IFCN standards for digital recording of clinical EEG. *Electroencephalogr Clin Neurophysiol*. 1998;106(3):259–261.
55. Tang Y, Norcia AM. An adaptive filter for steady-state evoked responses. *Electroencephalography and Clinical Neurophysiology/Evoked Potentials Section*. 1995;96(3):268–277.
56. Victor JD, Mast J. A new statistic for steady-state evoked potentials. *Electroencephalogr Clin Neurophysiol*. 1991;78(5):378–388.
57. Norcia AM, Tyler CW, Hamer RD, Wesemann W. Measurement of spatial contrast sensitivity with the swept contrast VEP. *Vis Res*. 1989;29(5):627–637.
58. Ales JM, Norcia AM. Assessing direction-specific adaptation using the steady-state visual evoked potential: Results from EEG source imaging. *J Vis*. 2009;9(7):8.
59. Norcia AM. Abnormal motion processing and binocularity: Infantile esotropia as a model system for effects of early interruptions of binocularity. *Eye*. 1996;10(2):259–265.
60. Virsu V, Rovamo J. Visual resolution, contrast sensitivity, and the cortical magnification factor. *Exp Brain Res*. 1979;37(3):475–494.
61. Zihl J, Von Cramon D, Mai N. Selective disturbance of movement vision after bilateral brain damage. *Brain*. 1983;106(2):313–340.
62. Hess RH, Baker CL, Zihl J. The "motion-blind" patient: low-level spatial and temporal filters. *J Neurosci*. 1989;9(5):1628–1640.
63. Zeki S. Cerebral akinetopsia (visual motion blindness) a review. *Brain*. 1991;114(2):811–824.
64. Jan JE, Groenvelde M, Sykanda AM, Hoyt CS. Behavioural characteristics of children with permanent cortical visual impairment. *Dev Med Child Neurol*. 1987;29(5):571–576.
65. Dutton GN, Calvert J, Ibrahim H, et al. Structured clinical history taking for cognitive and perceptual visual dysfunction and for profound visual disabilities due to damage to the brain in children. *Visual Impairment in Children Due to Damage to the Brain*. London, UK: Mac Keith Press; 2010 Jan 1:117–128.
66. Hou C, Good WV, Norcia AM. Validation study of VEP vernier acuity in normal-vision and amblyopic adults. *Invest Ophthalmol Vis Sci*. 2007;48(9):4070–4078.
67. Downie AL, Jakobson LS, Frisk V, Ushycky I. Periventricular brain injury, visual motion processing, and reading and spelling abilities in children who were extremely low birthweight. *J Int Neuropsychol Soc*. 2003;9:440–449.
68. Jakobson LS, Frisk V, Downie ALS. Motion-defined form processing in extremely premature children. *Neuropsychologia*. 2006;44(10):1777–1786.
69. MacKay TL, Jakobson LS, Ellemberg D, Lewis TL, Maurer D, Casiro O. Deficits in the processing of local and global motion in very low birthweight children. *Neuropsychologia*. 2005;43(12):1738–1748.
70. Benassi M, Bolzani R, Forsman L, Ådén U, Jacobson L, Giovagnoli S, Hellgren K. Motion Perception and Form Discrimination in Extremely Preterm School-Aged Children. *Child Develop*. 2018;89(6):e494–e506.
71. van Genderen M, Dekker M, Pilon F, Bals I. Diagnosing cerebral visual impairment in children with good visual acuity. *Strabismus*. 2012;20(2):78–83.
72. Atkinson J, Braddick O, Anker S, Curran W, Andrew R, Wattam-Bell J, Braddick F. Neurobiological models of visuospatial cognition in children with Williams syndrome: measures of dorsal-stream and frontal function. *Develop Neuropsychol*. 2003;23(1-2):139–172.
73. Chokron S, Kovarski K, Zalla T, Dutton GN. The inter-relationships between cerebral visual impairment, autism and intellectual disability. *Neurosci Biobehav Rev*. 2020;114:201–210.
74. Lueck AH, Dutton GN, Chokron S. Profiling children with cerebral visual impairment using multiple methods of assessment to aid in differential diagnosis. In: *Seminars in pediatric neurology* (Vol. 31, pp. 5–14). New York, NY: WB Saunders; 2019.
75. Bennett CR, Bauer CM, Bailin ES, Merabet LB. Neuroplasticity in cerebral visual impairment (CVI): Assessing functional vision and the neurophysiological correlates of dorsal stream dysfunction. *Neurosci Biobehav Rev*. 2020;108:171–181.

## APPENDIX A: TABLES 1A AND 1B. CLINICAL DATA FOR PATIENTS IN THIS STUDY

**Table 1. 1A:** Characteristics of the CVI participants including gestation, neurological diagnosis and key deficits, neuroradiology, visual acuity (Lea Symbol LogMAR Acuity) and ophthalmic findings. GMFCS = Gross Motor Function Classification System; ASD = autism spectrum disorder; IUGR = intra uterine growth restriction; HIE = hypoxic-ischemic encephalopathy; ADHD = attention deficit hyperactivity disorder; PVL = periventricular leukomalacia. **1B:** Eye findings of CVI participants. For other details see **Table 1A**. VA = visual acuity; OD = right eye; OS = left eye; OU = both eyes (VEP recordings were done under binocular viewing conditions); IAD = interocular acuity difference

(calculated OS-OD). All values are in LogMAR units. Ref Error = refractive error type as prescribed; ONH = optic nerve head; WNL = within normal limits (based on clinical examination).

Tables 2A and 2B. Summary of incidence of risk factors, neurological diagnoses, MRI scan results, associated neurological and ophthalmic findings in participants with CVI

TABLE 1A.

	M/F	Age	Birth	Neurological Diagnosis	MRI Brain Scan
1	F	5.75	Near term	16p13.11 deletion syndrome	Normal
2	F	6.80	Term	Cerebral palsy, GMFCS Level 2, asymmetric spastic diplegia	PVL
3	M	11.17	Term	Global Developmental Delay, ASD, mild neurodevelopmental deficits	Normal
4	M	5.91	Extreme preterm	Global developmental delay, ASD	PVL
5	F	12.51	Term	ASD, ADHD (came with diagnosis of CVI based on neurodevelopmental pediatrics DS difficulties)	not available
6	M	6.93	Near term	Neonatal meningitis	Normal
7	F	8.51	Term	Learning difficulties (moderate), ASD	Normal
8	F	5.78	Near term	Cerebral palsy, GMFCS Level 3, spastic diplegia	Not available
9	F	10.12	Extreme preterm	Cerebral palsy, GMFCS Level 1, left hemiplegia	Right frontal porencephalic cyst
10	F	10.18	Near term	Severe IUGR, dyspraxia, feeding difficulties, joint hypermobility	PVL
11	M	11.36	Term	Cerebral palsy, GMFCS Level 4, asymmetric spastic quadriplegia, right side more involved	Left fronto-parietal porencephalic cyst, hydrocephalus
12	M	8.50	Term	Cerebral palsy, GMFCS Level 2, mild neurodevelopmental deficits	Right fronto-parietal porencephalic cyst, white matter volume loss
13	F	11.57	Very preterm	Global Developmental Delay, moderate learning difficulties	PVL
14	F	10.66	Term	Cerebral palsy, GMFCS Level 1, right hemiplegia, mild learning difficulties, newborn HIE Grade 3	Bilateral occipital gliosis
15	M	9.72	Term	Newborn symptomatic hypoglycemia, normal gross neurology	Bilateral occipital gliosis
16	F	5.67	Term	Neurodevelopmental and congenital cardiac malformation syndrome, severe learning difficulties	PVL
17	F	12.14	Very preterm	Social communication difficulties, dyspraxia	Normal
18	M	4.52	Term	Cerebral palsy, GMFCS Level 1, right hemiplegia	Left fronto-parietal porencephalic cyst
19	M	10.82	Term	Neonatal hemorrhagic stroke, normal gross neurology	Right occipital gliosis
20	M	8.15	Preterm	Cerebral palsy, GMFCS Level 2, spastic diplegia	PVL
21	F	7.38	Term	IUGR, ASD	Normal
22	M	4.44	Term	ASD	Normal
23	F	11.56	Term	Cerebral palsy, GMFCS Level 2, right hemiplegia	Left temporo-parietal porencephalic cyst
24	M	9.09	Term	ASD	Bilateral dilated posterior horns lateral ventricles
25	F	8.32	Term	Meningitis, hydrocephalus	Hydrocephalus
26	M	14.53	Near term	Normal gross neurology	PVL
27	F	8.05	Very preterm	Cerebral palsy, GMFCS Level 3, spastic diplegia	PVL
28	F	4.41	Near term	Fine motor impairment, behavioral disorder	PVL
29	M	5.35	Term	Cerebral palsy, GMFCS Level 2, spastic diplegia, mild learning difficulties, neonatal meningitis	Bilateral occipital and parietal gliosis
30	F	8.81	Near term	Neonatal arterial ischemic stroke	Left parietal and temporal multicystic encephalomalacia
31	M	9.27	Term	Cerebral palsy, GMFCS Level 2, spastic diplegia, traumatic perinatal intracerebral hemorrhage	Right temporal and parietal multicystic encephalomalacia

TABLE 1B.

	VA OU	VA OD	VA OS	IAD	Amblyopia	Ref Error	Strabismus	ONH OD	ONH OS
1	0.00	0.00	0.10	-0.10	None	None	Exophoria	Mild pallor	WNL
2	0.10	0.10	0.70	-0.60	OS	Hyperopia & Astigmatism	Esotropia OS	WNL	WNL
3	0.00	0.80	0.00	0.80	OD	Hyperopia	Esotropia OD	WNL	WNL
4	0.20	0.30	0.30	0.00	OU	Myopia	None	WNL	WNL
5	0.00	0.00	0.00	0.00	None	None	None	WNL	WNL
6	0.10	0.40	0.10	0.30	OD	Hyperopia & Astigmatism	None	WNL	WNL
7	0.20	0.20	0.30	-0.10	OU	Hyperopia	Esotropia OS	WNL	WNL
8	0.20	0.40	0.20	0.20	OU; OD > OS	None	Exotropia OD	WNL	WNL
9	0.10	0.60	0.60	0.00	OU	Hyperopia	Esotropia OS	WNL	WNL
10	0.10	0.60	0.30	0.30	OU; OD > OS	Hyperopia & Astigmatism	Exotropia OD	WNL	WNL
11	0.20	0.40	0.20	0.20	OU; OD > OS	Hyperopia & Astigmatism	None	Mild pallor	Mild pallor
12	0.10	0.10	0.10	0.00	None	Hyperopia & Astigmatism	Esotropia	Mild pallor	Mild pallor
13	0.20	0.20	0.30	-0.10	OU	Hyperopia & Astigmatism	None	WNL	WNL
14	0.10	0.10	0.60	-0.50	OU; OS > OD	Hyperopia & Astigmatism	None	Hypoplasia	Hypoplasia
15	0.30	0.30	0.50	-0.20	OU; OS > OD	Hyperopia & Astigmatism	Exotropia	Mild pallor	Mild pallor
16	0.20	1.20	0.30	0.90	OU; OD > OS	Hyperopia & Astigmatism	Esotropia OD	Mild pallor	WNL
17	-0.10	-0.10	0.00	-0.10	None	None	Esotropia	WNL	WNL
18	0.40	0.40	0.50	-0.10	OU	Hyperopia & Astigmatism	Exotropia, hypertropia OS	WNL	WNL
19	0.00	0.00	0.00	0.00	None	None	Esotropia	Normal	Normal
20	0.10	0.10	0.10	0.00	OU	None	Right DVD, decompensated XP	Dragged disc	WNL
21	0.00	0.00	0.00	0.00	None	Hyperopia	None	Normal	Normal
22	0.10	0.10	0.10	0.00	None	None	Esotropia	Normal	Normal
23	0.10	0.10	0.80	-0.70	OS	Hyperopic Anisometropia	Esotropia	Mild pallor	Mild pallor
24	0.20	0.20	1.20	-1.00	OU; OS > OD	None	Esotropia, cataract OS	Normal	Hypoplasia
25	0.00	0.10	0.00	0.10	None	None	Exotropia	Normal	Normal
26	0.00	0.00	0.20	-0.20	OS	Myopia	Esotropia, hypertropia OS	Normal	Normal
27	0.20	0.20	0.20	0.00	OU	None	Exotropia	Normal	Normal
28	0.10	0.10	0.00	0.10	None	None	None	Poor views	Poor views
29	0.20	0.20	0.20	0.00	OU	None	Exotropia OS	Normal	Normal
30	0.10	0.10	0.10	0.00	None	None	Exotropia, DVD	Mild pallor	Mild pallor
31	0.20	0.20	0.20	0.00	OU	None	Intermittent exotropia	Mild pallor	Mild pallor

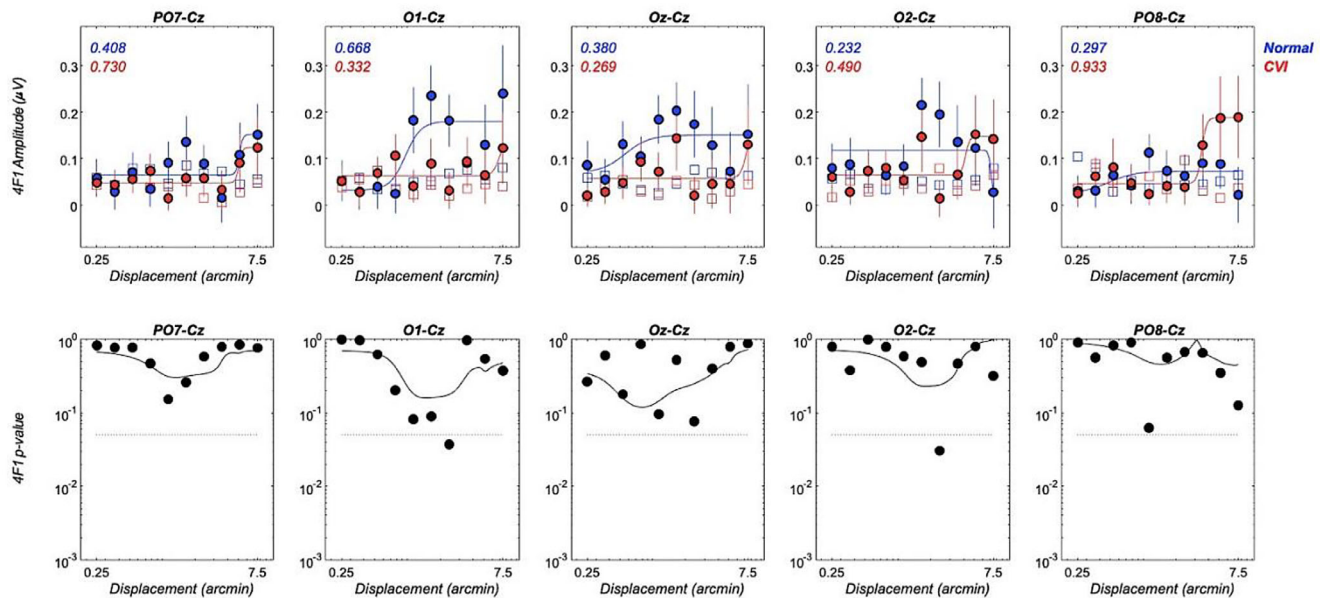
TABLE 2A.

<b>Birth history</b>	
At term	18
Prematurity	13
Near term (33 weeks to 36 + 6)	7
Preterm (32 wk + 6 days or less)	1
Very preterm (28 wk to < 32 wk)	3
Extreme preterm (< 28 wk)	2
<b>Neurological diagnosis (primary)</b>	
Cerebral palsy	12
Neonatal meningitis	1
Neonatal stroke	2
Neonatal hypoglycemia	1
Global developmental delay	3
Genetic disorder	2
Hydrocephalus (post meningitis)	1
Multiple diagnoses (from list above)	11
<b>Associated neurological findings</b>	
ASD	2
IUGR	2
ASD ADHD	1
Learning difficulties	1
Fine motor impairment, behavioral disorder	1
Dyspraxia, social communication difficulties	1
Normal gross neurology	1

TABLE 2B.

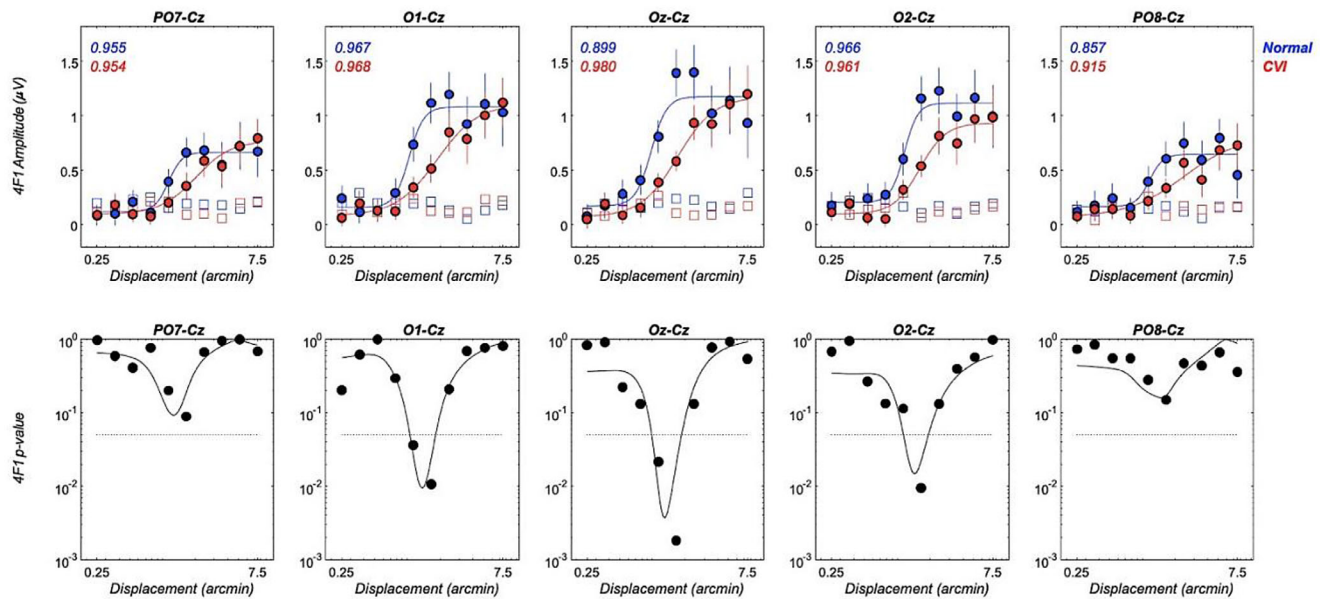
<b>MRI brain scan</b>	
PVL	9
Procephalic cyst	5
Occipital gliosis	4
Multicystic encephalomalacia	2
Hydrocephalus	1
Bilateral dilated posterior horns lateral ventricles	1
Normal	5
Not available	1
<b>Visual acuity</b>	
>/=0.00 Both eyes	8
0.10	11
0.20	10
0.30	1
0.40	1
<b>Refractive error</b>	
HM	15
Myopia	2
Emmetropic	14
<b>Strabismus</b>	
Esotropia	12
Exotropia	11
<b>Amblyopia</b>	23
<b>Optic nerve head</b>	
Unilateral pallor	2
Bilateral pallor	6

**APPENDIX B: FOURTH HARMONIC RESPONSE TO ABSOLUTE MOTION**



**FIGURE B.** Absolute Motion. TOP: Group average response functions for absolute motion response (displacement) at 4F fast-jitter harmonic response. VEP amplitude versus displacement size is plotted for each of five electrodes for children with CVI (red) and age-matched neurotypical controls (blue). Open squares indicate the noise-level during the trial measured at frequencies adjacent to the response frequency. BOTTOM: Each figure plots the result of two-sample *t*-tests for between-group differences at each sweep step. Compare to similar responses at second harmonic in Results section: Absolute motion.

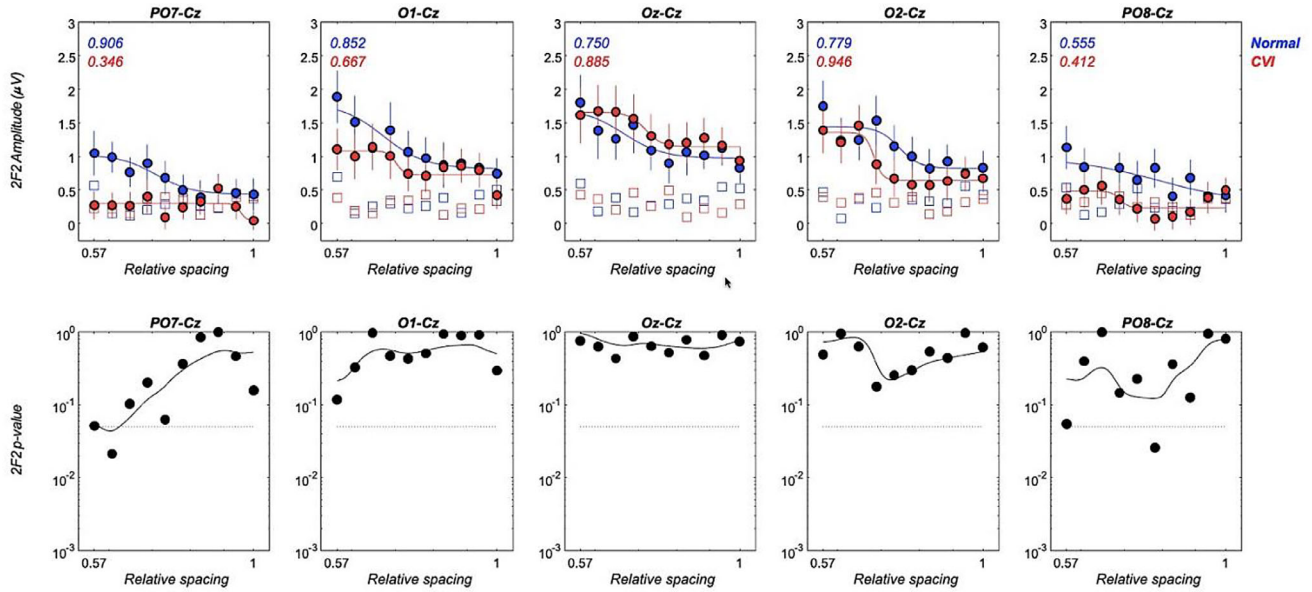
**APPENDIX C: FOURTH HARMONIC RESPONSE TO RELATIVE MOTION**



**FIGURE C.** Relative Motion. TOP: Group average response functions for relative motion response (displacement) at 4F harmonic response observed in the vernier paradigm. VEP amplitude versus displacement size is plotted for each of five electrodes (the three central electrodes show the best responses) for children with CVI (red) and age-matched neurotypical controls (blue). Open squares indicate the noise-level during the trial measured at frequencies adjacent to the response frequency. BOTTOM: Each figure plots the result of two-sample *t*-tests for between-group differences at each sweep step with significant differences between children with CVI and typically developing controls. Compare to significant responses also at second harmonic in Results section: Relative motion.



**APPENDIX D: THE 2F2 HARMONIC RESPONSE TO ROTARY MOTION**



**FIGURE D.** Rotary Motion TOP: Group average response functions for rotary motion (2F2) response. VEP amplitude versus density of surrounding Gabor patches is plotted for each of five electrodes for children with CVI (red) and age-matched neurotypical controls (blue). Open squares indicate the noise-level during the trial measured at frequencies adjacent to the response frequency. BOTTOM: Figure plots the result of two-sample *t*-tests for between-group differences at each sweep step. Dotted line is  $P = 0.05$  significance criterion. See Results section: Rotary Motion for responses at fourth harmonic.